PAPER • OPEN ACCESS

Subradiance-protected excitation transport

New Journal of Physics
The open access journal at the forefront of physics

Deutsche Physikalische Gesellschaft DPG
IOP Institute of Physics

Published in partnership with: Deutsche Physikalische Gesellschaft and the Institute of Physics

OPEN ACCESS

RECEIVED
13 May 2019

REVISED
26 June 2019

ACCEPTED FOR PUBLICATION
12 July 2019

PUBLISHED
30 July 2019

PAPER

Subradiance-protected excitation transport

Jemma A Needham[1,2], **Igor Lesanovsky**[1,2] **and Beatriz Olmos**[1,2]

[1] School of Physics and Astronomy, The University of Nottingham, Nottingham, NG7 2RD, United Kingdom
[2] Centre for the Mathematics and Theoretical Physics of Quantum Non-equilibrium Systems, The University of Nottingham, Nottingham, NG7 2RD, United Kingdom

E-mail: beatriz.olmos-sanchez@nottingham.ac.uk

Keywords: light–matter interactions, excitation transport, open quantum systems

Abstract

We explore excitation transport within a one-dimensional chain of atoms where the atomic transition dipoles are coupled to the free radiation field. When the atoms are separated by distances smaller or comparable to the wavelength of the transition, the exchange of virtual photons leads to the transport of the excitation through the lattice. Even though this is a strongly dissipative system, we find that the transport is subradiant, that is, the excitation lifetime is orders of magnitude longer than the one of an individual atom. In particular, we show that a subspace of the spectrum is formed by subradiant states with a linear dispersion relation, which allows for the dispersionless transport of wave packets over long distances with virtually zero decay rate. Moreover, the group velocity and direction of the transport can be controlled via an external uniform magnetic field while preserving its subradiant character. The simplicity and versatility of this system, together with the robustness of subradiance against disorder, makes it relevant for a range of applications such as lossless energy transport and long-time light storage.

1. Introduction

An ensemble of emitters couples collectively to a common electromagnetic bath, as was already investigated theoretically in the seminal papers of Dicke, Lehmberg and Agarwal in the 1950s and 70s [1–3]. Here, the exchange of virtual photons results in induced dipole–dipole interactions [4–6] and collective Lamb and Lorentz–Lorenz shifts [7–13]. Moreover, the emission of photons into the bath takes place at a rate much faster or slower (so-called super- and subradiance, respectively) than the single atom decay rate [14–21]. This cooperative behavior is featured both in dense ensembles, where the interparticle separations are comparable to the wavelength of the scattered light, and in dilute ones with a very large number of emitters. Super- and subradiance have been observed experimentally not only in atomic gases, but also in QED circuits [22, 23], metamaterial arrays [24], and quantum dots [25–27]. This collective atom-light coupling has found a variety of applications such as storage of light via the preparation of subradiant states through phase-imprinting protocols [28–38], topologically protected transport of excitations [39, 40], or efficient long-range energy transport [41–46].

In this paper, we show that it is possible to realize subradiance-protected transport of a wave packet through a dense atomic chain with lifetimes many orders of magnitude longer than the one of an individual atom. This is achieved by maximizing the overlap of the wave packet with a subradiant manifold of states that possess a linear dispersion relation. Further control over the transport can be attained by effectively changing the orientation of the transition dipoles via an external uniform magnetic field. In particular, we show that the group velocity of the wave packet can be brought close to zero while preserving its long lifetime. Finally, we analyze the effect of disorder, which arises from the width of the external wavefunction of the atoms in each lattice trap and is inevitable in a realistic experimental scenario. Even though this can lead to the suppression of the transport of the wave packet due to localization [47, 48], we find that the subradiant character of the dynamics is robust against the presence of disorder [49, 50].

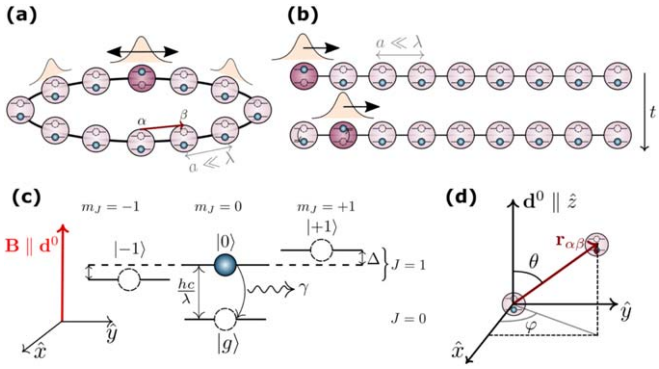

Figure 1. The system. We consider a one-dimensional chain of atoms with nearest neighbor separation a in (a) a ring and (b) a linear chain with open boundary conditions. The wave packet that contains the excitation is transported via dipole–dipole interactions induced by the collective coupling to the radiation field at zero temperature. (c) We consider the following internal atomic levels in each atom: a ground state $|g\rangle$ and three degenerate excited states $|-1\rangle$, $|0\rangle$, $|+1\rangle$. The degeneracy is lifted by the shift of $|\pm1\rangle$ by $\pm\Delta = \pm\mu_B g|\mathbf{B}|$ when an external uniform magnetic field $\mathbf{B}$ is aligned with the dipole moment $\mathbf{d}^0$ of the $|g\rangle \rightarrow |0\rangle$ transition (quantization axis). (d): The polar angle θ of $\mathbf{r}_{\alpha\beta}$ (separation between the αth and βth atoms) controls the strength of the interactions and the collective character of the dissipation.

2. Interaction between the atoms and the radiation field

2.1. Master equation

We consider an ensemble of N atoms at positions $\mathbf{r}_\alpha$ with $\alpha = 1, \ldots, N$, each one tightly trapped in the sites of a one-dimensional lattice with lattice constant a (see figures 1(a) and (b)). The internal degrees of freedom of each atom are considered as a generic $J = 0 \rightarrow 1$ transition, with a single ground state $|g\rangle$ and three degenerate excited states $|-1\rangle$, $|0\rangle$ and $|+1\rangle$. The energy difference between the ground and excited states is denoted by $\hbar\omega = hc/\lambda$, where λ is the wavelength of the transition. We choose the transition dipole moment $\mathbf{d}^0$ of the $|g\rangle \rightarrow |0\rangle$ transition to be aligned with the quantization axis (z-axis) (figure 1(c)).

The atoms are in contact with the radiation field, which we model as a thermal bath at zero temperature, whose degrees of freedom are traced out. Within the Born–Markov and secular approximations [1–3], the master equation for the dynamics of the internal degrees of freedom encoded in the reduced density matrix ρ yields [51]

$$\dot{\rho}(t) = -\frac{\mathrm{i}}{\hbar}[H, \rho] + \mathcal{D}(\rho). \tag{1}$$

The Hamiltonian H describes the coherent long-ranged exchange of virtual photons among the atoms and is given by

$$H = \hbar \sum_{\alpha \neq \beta} \mathbf{d}'_\alpha \cdot \bar{V}_{\alpha\beta} \mathbf{d}_\beta, \tag{2}$$

where $\mathbf{d}_\alpha = \begin{pmatrix} d_\alpha^{+1} & d_\alpha^0 & d_\alpha^{-1} \end{pmatrix}^T$ and $\mathbf{d}'_\alpha = \begin{pmatrix} d_\alpha^{+1\dagger} & d_\alpha^{0\dagger} & d_\alpha^{-1\dagger} \end{pmatrix}^T$ with the atomic lowering and raising operators defined as $d_\alpha^m = |g\rangle_\alpha \langle m|$ and $d_\alpha^{m\dagger} = |m\rangle_\alpha \langle g|$, respectively, for $m = -1, 0, +1$ and $\alpha = 1, \ldots, N$. The coherent exchange rate between two atoms α and β is represented by the coefficient matrix

$$\bar{V}_{\alpha\beta} = \frac{3\gamma}{8} \begin{pmatrix} V_{11} & -V_{10}^* & V_{+-}^* \\ -V_{10} & V_{00} & V_{10}^* \\ V_{+-} & V_{10} & V_{11} \end{pmatrix}, \tag{3}$$

with

$$V_{11} = (2 - 3\sin^2\theta)\left(\frac{\sin\kappa}{\kappa^2} + \frac{\cos\kappa}{\kappa^3}\right) - (2 - \sin^2\theta)\frac{\cos\kappa}{\kappa}$$

$$V_{10} = \frac{1}{\sqrt{2}} \sin 2\theta \mathrm{e}^{\mathrm{i}\varphi}\left[\frac{\cos\kappa}{\kappa} - 3\left(\frac{\sin\kappa}{\kappa^2} + \frac{\cos\kappa}{\kappa^3}\right)\right]$$

$$V_{00} = 2\left[(1 - 3\cos^2\theta)\left(\frac{\sin\kappa}{\kappa^2} + \frac{\cos\kappa}{\kappa^3}\right) - \sin^2\theta\frac{\cos\kappa}{\kappa}\right]$$

$$V_{+-} = \sin^2\theta \mathrm{e}^{2\mathrm{i}\varphi}\left[3\left(\frac{\sin\kappa}{\kappa^2} + \frac{\cos\kappa}{\kappa^3}\right) - \frac{\cos\kappa}{\kappa}\right].$$

All exchange rates between the internal states are proportional to the single-atom decay rate γ and depend on the reduced distance between the two atoms $\kappa = 2\pi r_{\alpha\beta}/\lambda$. Here, $r_{\alpha\beta} = |\mathbf{r}_{\alpha\beta}|$ is the modulus of the separation between the two atoms $\mathbf{r}_{\alpha\beta} = \mathbf{r}_\alpha - \mathbf{r}_\beta$, and θ and φ are the angles between $\mathbf{r}_{\alpha\beta}$ and the transition dipole moment $\mathbf{d}^0$ and the x-axis, respectively (see figure 1(d)).

For small values of κ (near-field) the exchange interactions (3) decay approximately as $1/\kappa^3$. Here, for a fixed value of κ, both the strength and sign of the interactions can be tuned by changing the angle θ (e.g. $V_{00} \approx 2(1 - 3\cos^2\theta)/\kappa^3$). Control over this angle and, hence, the interactions, is obtained by applying a uniform magnetic field $\mathbf{B} = (B_x, B_y, B_z)$, represented in the master equation (1) by substituting $H \rightarrow H + H_\Delta$, with

$$H_\Delta = \sum_{\alpha=1}^{N} \mathbf{d}'^{*}_{\alpha} \cdot \bar{\Delta}_{\alpha\alpha} \mathbf{d}_\alpha. \tag{4}$$

Here, the matrix $\bar{\Delta}_{\alpha\alpha}$ reads

$$\bar{\Delta}_{\alpha\alpha} = \mu_B g \begin{pmatrix} B_z & \frac{B_x - iB_y}{\sqrt{2}} & 0 \\ \frac{B_x + iB_y}{\sqrt{2}} & 0 & \frac{B_x - iB_y}{\sqrt{2}} \\ 0 & \frac{B_x + iB_y}{\sqrt{2}} & -B_z \end{pmatrix}, \tag{5}$$

with μ_B being the Bohr magneton and g the Landé g-factor.

The second term of the master equation (1) represents the dissipation via incoherent emission of photons into the radiation field and it is given by

$$\mathcal{D}(\rho) = \sum_{\alpha,\beta} \left(\mathbf{d}_\alpha \cdot \bar{\Gamma}_{\alpha\beta} \rho \mathbf{d}'^{*}_{\beta} - \frac{1}{2} \{ \mathbf{d}'^{*}_{\alpha} \cdot \bar{\Gamma}_{\alpha\beta} \mathbf{d}_\beta, \rho \} \right). \tag{6}$$

The coefficient matrix $\bar{\Gamma}_{\alpha\beta}$ encodes the dissipative couplings between the atoms and has a similar structure to the coherent interaction matrix:

$$\bar{\Gamma}_{\alpha\beta} = \frac{3\gamma}{4} \begin{pmatrix} \Gamma_{11} & -\Gamma_{10}^* & \Gamma_{+-}^* \\ -\Gamma_{10} & \Gamma_{00} & \Gamma_{10}^* \\ \Gamma_{+-} & \Gamma_{10} & \Gamma_{11} \end{pmatrix}, \tag{7}$$

with

$$\begin{aligned}
\Gamma_{11} &= (2 - \sin^2\theta) \frac{\sin\kappa}{\kappa} + (2 - 3\sin^2\theta) \left(\frac{\cos\kappa}{\kappa^2} - \frac{\sin\kappa}{\kappa^3} \right) \\
\Gamma_{10} &= \frac{1}{\sqrt{2}} \sin 2\theta e^{i\varphi} \left[-\frac{\sin\kappa}{\kappa} - 3 \left(\frac{\cos\kappa}{\kappa^2} - \frac{\sin\kappa}{\kappa^3} \right) \right] \\
\Gamma_{00} &= 2 \left[\sin^2\theta \frac{\sin\kappa}{\kappa} + (1 - 3\cos^2\theta) \left(\frac{\cos\kappa}{\kappa^2} - \frac{\sin\kappa}{\kappa^3} \right) \right] \\
\Gamma_{+-} &= \sin^2\theta e^{2i\varphi} \left[\frac{\sin\kappa}{\kappa} + 3 \left(\frac{\cos\kappa}{\kappa^2} - \frac{\sin\kappa}{\kappa^3} \right) \right].
\end{aligned}$$

The atoms couple to the radiation field as a collective and not as individuals. As a consequence, the decay rates in the system differ significantly from those of single emitters [1–3], with some being much larger and others much smaller than the single-atom decay rate γ (corresponding to so-called superradiant and subradiant emission modes, respectively). This collective character becomes more pronounced for small reduced distances κ, i.e. small ratios a/λ, reaching regimes where some of the radiation modes are almost completely dark (with virtually zero decay rate). The population of these subradiant modes is the mechanism that allows for the prolonged storage of light in the atomic system.

2.2. Dynamics in the single excitation sector

Throughout, we will assume that the initial state contains a single excitation localized over a few lattice sites of the chain (figures 1(a) and (b)). This single excitation (in one of the three states $|-1\rangle$, $|0\rangle$, or $|+1\rangle$) is transported

via the exchange interactions given by H (which conserve the number of excitations), while the action of dissipation can only decrease the number of excitations to zero. Thus, the dynamics can be described in a truncated space formed by the many-body ground state $|G\rangle \equiv |g\rangle_1 \otimes |g\rangle_2 ... \otimes |g\rangle_N$ and the single-excitation states $|e^m\rangle_\alpha \equiv |g\rangle_1 \otimes |g\rangle_2 ... |m\rangle_\alpha ... \otimes |g\rangle_N$, for all $\alpha = 1 ... N$ and $m = -1, 0, +1$. Here, the density matrix takes the form

$$\rho = \begin{pmatrix} \rho_{GG} & \boldsymbol{\rho}_{Ge} \\ \boldsymbol{\rho}_{eG} & \bar{\rho}_{ee} \end{pmatrix}, \tag{8}$$

where $\rho_{GG} = \langle G|\rho|G\rangle$, $\boldsymbol{\rho}_{Ge} = \langle G|\rho|\mathbf{e}\rangle$, $\boldsymbol{\rho}_{eG} = \langle \mathbf{e}|\rho|G\rangle$, and $\bar{\rho}_{ee} = \langle \mathbf{e}|\rho|\mathbf{e}\rangle$, with $|\mathbf{e}\rangle$ being a row vector containing all single-excitation states $|e^m\rangle_\alpha$.

At this point it is convenient to rewrite the master equation (1) as

$$\dot{\rho} = -\frac{\mathrm{i}}{\hbar}[\mathcal{H}_{\mathrm{eff}}, \rho] + \sum_{\alpha,\beta} \mathbf{d}_\alpha \cdot \bar{\Gamma}_{\alpha\beta}\rho\mathbf{d}'_\beta, \tag{9}$$

with the effective (non-Hermitian) Hamiltonian

$$\mathcal{H}_{\mathrm{eff}} = \hbar\sum_{\alpha,\beta} \mathbf{d}'_\alpha \cdot \left(\bar{V}_{\alpha\beta} - \mathrm{i}\frac{\bar{\Gamma}_{\alpha\beta}}{2} + \frac{1}{\hbar}\bar{\Delta}_{\alpha\beta}\right)\mathbf{d}_\beta, \tag{10}$$

where $\bar{V}_{\alpha\alpha} = 0$ and $\bar{\Delta}_{\alpha\beta} = \bar{\Delta}_{\alpha\alpha}\delta_{\alpha\beta}$. Here, using that within the truncated subspace $d_\beta^{m\dagger}|\mathbf{e}\rangle = 0$, one easily obtains that the time-evolution of the elements of $\bar{\rho}_{ee}$ (a $3N \times 3N$ matrix) is decoupled from the dynamics of the remaining elements (see appendix), obeying the equation

$$\dot{\bar{\rho}}_{ee} = -\frac{\mathrm{i}}{\hbar}[H_{\mathrm{eff}}, \bar{\rho}_{ee}], \tag{11}$$

with

$$H_{\mathrm{eff}} = \hbar\left(\bar{V} - \mathrm{i}\frac{\bar{\Gamma}}{2}\right) + \bar{\Delta}. \tag{12}$$

Here, $\bar{V}$, $\bar{\Gamma}$, and $\bar{\Delta}$, are $3N \times 3N$ matrices whose components for $\alpha, \beta = 1, \ldots, N$ are given by equations (3), (7) and (5), respectively.

We will consider the initial state in all cases as a pure state, and hence $\bar{\rho}_{ee} = |\psi(t)\rangle\langle\psi(t)|$ with

$$|\psi(t)\rangle = \sum_{m=\pm1,0}\sum_{\alpha=1}^{N} c_\alpha^m(t)|e^m\rangle_\alpha, \tag{13}$$

where $c_\alpha^m(t)$ is the probability amplitude of the αth atom being excited to the $|m\rangle$ state. The state (13) evolves under the non-Hermitian Hamiltonian H_{eff}. While the equation (9) for the density matrix is trace preserving, $\mathrm{Tr}[\rho] = 1$, the value of ρ_{GG} increases over time due to the dissipative dynamics. Therefore, the survival probability, i.e. the probability for not emitting a photon into the radiation field, is given by the norm of the wave function

$$P_{\mathrm{sur}}(t) = \sum_{\alpha=1}^{N}\sum_{m=\pm1,0}|c_\alpha^m(t)|^2, \tag{14}$$

which decreases as a function of time.

The instantaneous photon emission rate, also called activity, is given by

$$\langle K(t)\rangle = \sum_{\alpha,\beta}\langle \mathbf{d}'_\alpha \cdot \bar{\Gamma}_{\alpha\beta}\mathbf{d}_\beta\rangle. \tag{15}$$

A value of the activity larger (smaller) than the single atom decay rate γ for a state with large excitation density is indicative of collective superradiant (subradiant) behavior of the photon emission. For example, for a single two-level atom excited to $|e\rangle$, the activity at $t = 0$ is simply given by $\langle K(0)\rangle = \gamma$, i.e. the single atom emission rate. Extending this system now to $N = 2$ two-level atoms, with an initial state that is either a symmetric (+) or anti-symmetric (−) superposition of each atom being excited $|\psi(0)\rangle = \frac{1}{\sqrt{2}}(|e\rangle_1 \pm |e\rangle_2)$, the initial activity is $\langle K(0)\rangle = \frac{1}{2}(\Gamma_{11} \pm \Gamma_{12} \pm \Gamma_{21} + \Gamma_{22})$. In the limit of non-interacting atoms, the coefficients tend towards $\Gamma_{\alpha\alpha} = \gamma$ and $\Gamma_{\alpha\neq\beta} = 0$. The activity in this case is therefore $\langle K(0)\rangle = \gamma$, as one would expect; the atomic

separation is large enough so that the atoms behave as independent emitters. Conversely, when $a \to 0$, all coefficients are $\Gamma_{\alpha\beta} \approx \gamma$. A symmetric initial state then has associated a large activity, $\langle K(0)\rangle = 2\gamma$, while for the anti-symmetric state it yields $\langle K(0)\rangle = 0$, hence demonstrating cooperative effects in the form of super- and subradiant emission rates.

3. Subradiant transport on a ring lattice

First, we focus on a ring lattice, as illustrated in figure 1(a) [35–37]. Here, the matrices $\bar{V}$ and $\bar{\Gamma}$ are symmetric circulant due to the periodic boundary conditions such that, for each orientation of the transition dipole m, the simultaneous eigenstates for both matrices are given by the plane waves

$$|k_m\rangle = \frac{1}{\sqrt{N}} \sum_{\alpha=1}^{N} e^{i\frac{2\pi}{N}(\alpha-1)(k-q)} |e^m\rangle_\alpha, \tag{16}$$

with $k = -\lfloor N/2 \rfloor, \ldots \lfloor (N-1)/2 \rfloor$ and $q = \lfloor N/2 \rfloor$. For illustration purposes, we will consider in the following the case where only the $|0\rangle$ state is excited initially, and where the ring plane is perpendicular to the dipole moment $\mathbf{d}^0$ (i.e. $\theta = \pi/2$). Here, both the coherent and incoherent couplings between $|0\rangle$ and $|\pm 1\rangle$ vanish ($V_{10} = 0$ and $\Gamma_{10} = 0$ in equations (3) and (7)), and hence the dynamics is determined solely by V_{00} and Γ_{00}. The initial state can be written as

$$|\psi(0)\rangle = \sum_\alpha c_\alpha^0 |e^0\rangle_\alpha = \frac{1}{\sqrt{N}} \sum_k c_k |k_0\rangle, \tag{17}$$

where the coefficients c_α^0 and c_k represent the probability amplitude distribution of the initial state in real and momentum space, respectively. Conversely, the time-evolved state takes the form

$$|\psi(t)\rangle = \frac{1}{\sqrt{N}} \sum_k c_k e^{-i\left(V_k - i\frac{\Gamma_k}{2}\right)t} |k_0\rangle, \tag{18}$$

where V_k and Γ_k are the eigenvalues of the matrices $\bar{V}$ and $\bar{\Gamma}$, respectively. Note that the collective character of the dissipation is reflected here in the decay rates Γ_k, which are either larger or smaller than the single atom decay rate γ, corresponding to $|k_0\rangle$ having superradiant or subradiant character, as illustrated in figure 2(a), while V_k represents the energy of the corresponding mode.

Let us start by considering the initial state to be $|e^0\rangle_1$, i.e. an excitation localized on a single site of the lattice such that $c_\alpha^0 = \delta_{\alpha 1}$. This state can be written as a symmetric superposition of all plane waves (16), i.e.

$$|\psi(0)\rangle = \frac{1}{\sqrt{N}} \sum_k |k_0\rangle, \tag{19}$$

and its time-evolution is then given by

$$|\psi(t)\rangle = \frac{1}{\sqrt{N}} \sum_k e^{-i\left(V_k - i\frac{\Gamma_k}{2}\right)t} |k_0\rangle. \tag{20}$$

This dynamics is depicted in figure 2(b), where we observe that the initial wave packet splits into two that travel in opposite directions. These wave packets disperse quickly due to the nonlinearity of V_k as a function of $p(k) = 2\pi k/(Na)$ (see figure 2(a)). More importantly, the superradiant components (with large Γ_k) decay very fast and only the subradiant ones remain populated. This is seen in figure 2(c), which shows a plateau in the survival probability P_{sur}, and near-zero emission rate $\langle K\rangle$ after a rapid initial decay. The height of the plateau of P_{sur} is approximately given by the number of subradiant eigenstates (much larger than the number of superradiant ones, as can be seen in figure 2(a)) divided by the total number of modes N[3]. For a fixed value of a/λ, this ratio remains almost constant when increasing the number of atoms N. For a fixed size of the system N, on the other hand, reducing a/λ increases the relative number of subradiant eigenstates and hence the survival probability, as can be seen in figure 2(d). In all cases considered, the lifetime of the excitation is dramatically longer than in the case of a single atom.

As can be observed in figures 2(a) and 3(a), the dispersion relation in the subradiant part of the spectrum is approximately linear (excluding the states with momentum $p(k)$ close to $\pm\pi/a$ and near the superradiant region). Therefore, one can expect to have lossless-propagating wave packets with a constant group velocity (given by the gradient of V_k) without dispersing. We illustrate this by initializing the system with a Gaussian wave packet centered in momentum space at $p(k_s)$ (center of the linear dispersion manifold) and width σ_k small enough to ensure that most components of the wave packet are located in the linear dispersion regime (see blue solid line in figure 3(a)):

[3] Note that this approximation only holds for small enough values of a/λ. As this ratio is increased, the decay rate Γ_k of the subradiant states get closer to γ and hence the plateau only holds for a small period of time τ, given by the difference between $1\,\Gamma_k$ and $1\,\Gamma_{k+1}$.

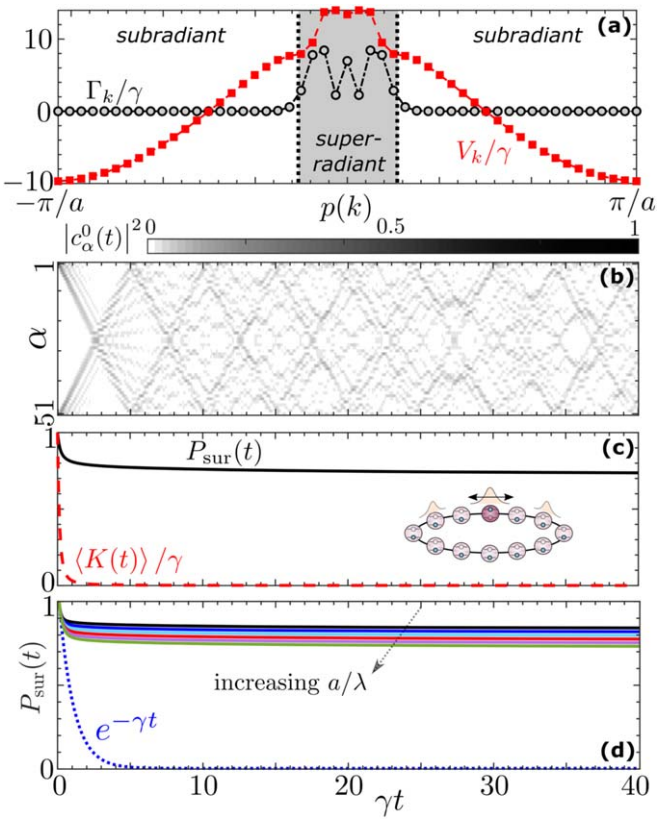

Figure 2. Subradiance on a ring. (a): Decay rates Γ_k and energy V_k of each mode $|k_0\rangle$ as a function of the momentum $p(k) = 2\pi k/(Na)$ for a for lattice formed by $N = 51$ atoms and $a/\lambda = 0.08$. The gray area indicates states which are superradiant, i.e. $\Gamma_k > \gamma$. (b) Excitation probability $|c_\alpha^0(t)|^2$ at site α as a function of time given by (20) for an initial excitation on site $\alpha = 1$. (c) Probability of survival of the initial excitation $P_{\rm sur}$ (black solid line) and activity $\langle K\rangle$ (red dashed line) as a function of time. (d) Survival probability as a function of time varying the ratio a/λ from 0.05 to 0.1. The exponential decay of a single atom (dashed blue line) is shown for comparison.

$$|\psi(0)\rangle = \frac{1}{\sqrt{\sqrt{2\pi}\,\sigma_k}} \sum_k \mathrm{e}^{-\frac{[p(k)-p(k_s)]^2}{4\sigma_k^2}} |k_0\rangle. \tag{21}$$

In real space this is also a Gaussian wave packet

$$|\psi(0)\rangle = \sqrt{\frac{\sigma_k}{\sqrt{2\pi}}} \sum_\alpha \mathrm{e}^{-\mathrm{i}p(k_s)a(\alpha-1)} \mathrm{e}^{-\frac{[\alpha-1]^2a^2}{4/\sigma_k^2}} |e^0\rangle_\alpha, \tag{22}$$

whose probability distribution is sketched on the left-hand side of figure 3(b). Here, it is shown that such wave packets travel indeed without appreciable dispersion around the ring. Moreover, the lifetime of the excitation is extremely long: its effective decay rate $\Gamma_{\rm eff}$ is six orders of magnitude smaller than the single atom decay rate γ. A similar reduction of the decay rate $\Gamma_{\rm eff}$ is also achieved for different system sizes N and ratios a/λ, as it can be observed in figure 3(c).

4. Finite linear chain: storage and transport control via magnetic field switching

In this section we will focus on the control of the subradiant excitation transport and storage on a linear one-dimensional chain with open boundary conditions, as depicted in figure 4(a) [22, 31, 33, 34]. We consider the initial state to be $|e^0\rangle_1$, representing one excitation at the leftmost site with the rest of the atoms in the ground state. We further assume that a uniform magnetic field $\mathbf{B}$ is applied perpendicularly to the chain (which lies on the y-axis) and parallel to $\mathbf{d}^0$, such that $\theta = \pi/2$.

The initial excitation is transported to the right of the chain via the dipole–dipole interactions (see figure 4(b)) until it reaches the other edge of the lattice and bounces back. As in the case of the ring, the excitation quickly disperses, and acquires a subradiant character when reaching the bulk of the chain (see figure 4(c)). However, as the excitation reaches the other edge, the survival probability decays faster, accompanied by an increase of the activity. Analogously with the case of the ring, the height of the plateau in $P_{\rm sur}$ can be increased by reducing the ratio a/λ, as illustrated in figure 4(d). Here, in order to facilitate the comparison, the time is scaled

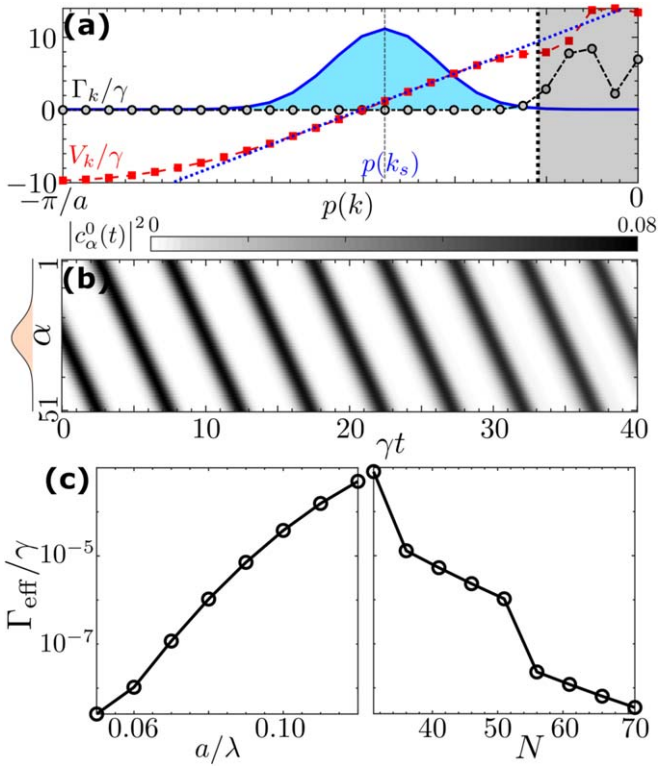

Figure 3. Subradiance-protected wave packet. (a) Decay rates Γ_k and energy V_k of each mode $|k_0\rangle$ as a function of the momentum $p(k) = 2\pi k/(Na)$ for a lattice formed by $N = 51$ atoms and $a/\lambda = 0.08$. The initial wave packet's probability distribution in momentum space (blue solid line) is centered at $p(k_s) \approx -0.43\pi/a$, with width $\sigma_k = \pi/(16a)$. Here, the dispersion relation is approximately linear (blue dashed line to guide the eye). (b) Excitation probability $|c^0_\alpha(t)|^2$ at site α as a function of time. The initial wave packet's probability distribution in real space is sketched on the left. (c) Effective decay rate $\Gamma_{\rm eff}/\gamma$ of the excitation for $N = 51$ as a function of a/λ (left panel) and for $a/\lambda = 0.08$ as a function of N (right panel).

by $t_{\rm pl}$, which is approximately the time that the excitation takes to reach the middle of the chain (inversely proportional to the nearest neighbor exchange rate).

Since the excitation has almost zero decay rate within the bulk of the chain, its lifetime is ultimately limited by the time it takes for it to reach the other boundary, i.e. by size of the system and the value of the exchange interactions. One can ask, thus, whether it is possible to freeze the transport of the wave packet and confine it in the subradiant states of the bulk. This can indeed be done by adiabatically changing the direction of the external magnetic field, exploiting that the strength and sign of the exchange interactions depends on the angle between the transition dipole moment $\mathbf{d}^0$ and the direction of the separation between the atoms θ.

Let us illustrate this protocol via an example depicted in figure 5 for the same parameters used in figure 4. At $t = 0, \theta = \pi/2$, such that the nearest neighbor interactions are larger than the single atom decay rate γ (as shown in figure 5(c), orange line), and make the excitation propagate into the bulk (see figures 5(a) and (b)). When the activity reaches a minimum at $t = t_{\rm min}$, the direction of the magnetic field is changed within the yz-plane. This switch is done adiabatically, such that it is followed by the transition dipole moment of the excitation (i.e. the switching time $\tau \gg 1/\Delta$), but quickly enough to keep the excitation from leaving the bulk of the lattice, such that τ should generally be kept smaller than $1/\gamma$ (depending also on the size of the lattice and the ratio a/λ). The change of the magnetic field direction is mathematically equivalent to a rotation of the angle θ between the quantization axis and the chain from its initial value $\theta_{\rm in} = \pi/2$ to a final value $\theta_{\rm f}$, which leads in turn to modified interactions. In particular, in order to slow down the excitation transport in the bulk, we fix the final value such that the nearest-neighbor interaction coefficient is zero, $V_{00}(a, \theta_{\rm f}) = 0$ (see figure 5(c), blue line). While this change does not freeze the excitation transport entirely due to the non-zero values of the exchange rates beyond nearest neighbors, it does slow it down notably, as one can see in figure 5(a). Most importantly, the subradiant character of the propagation is preserved, reflected in a constant survival probability $P_{\rm sur}$ and vanishing activity, as shown in figure 5(b).

The versatility of the system using the change in the magnetic field direction is further illustrated in figure 5(d). Here, we show an example where several changes in the direction of the magnetic field allow to

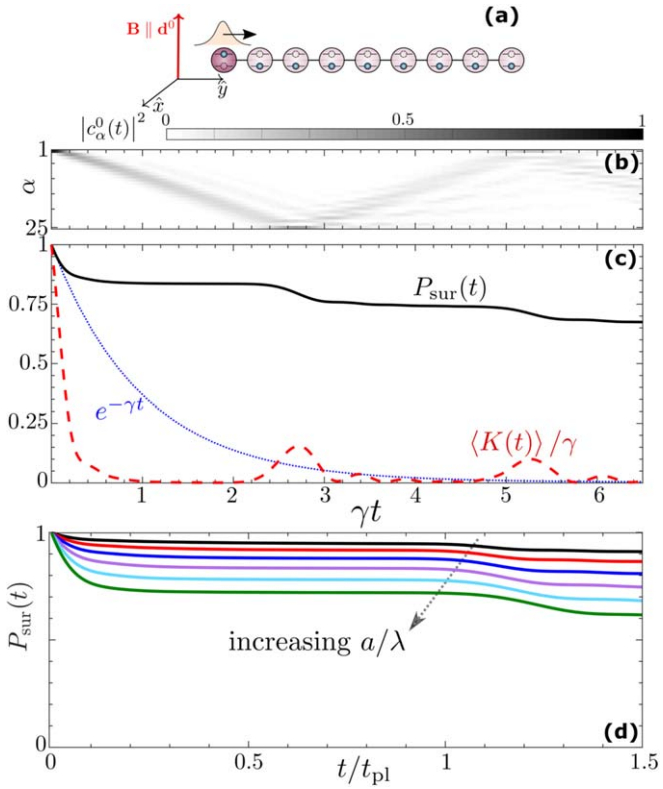

Figure 4. Subradiance on a linear chain. (a) Dynamics of a single excitation, initially on the leftmost atom ($\alpha = 1$) with transition dipole moment perpendicular to the chain, propagating through the chain of $N = 25$ atoms with $a/\lambda = 0.08$. (b) Excitation probability $|c_\alpha^0(t)|^2$ at each site α as a function of time. (c) Survival probability $P_{\rm sur}(t)$ (solid black) and activity $\langle K(t)\rangle/\gamma$ (dashed red) as a function of time. The blue dotted line represents the survival probability in a non-interacting case. (d) Survival probability as a function of time, varying the ratio a/λ from 0.05 to 0.1. The time is given in units of $t_{\rm pl}$ (see main text).

switch the direction of travel of the excitation. Most importantly, the activity remains close to zero throughout all of these changes, as long as the excitation stays in the bulk of the chain.

5. Disorder

Finally, we briefly consider the effect of disorder on the subradiant transport discussed in the previous sections. In particular, we consider the disorder introduced due to the finite width of the external wavefunction of each atom, which we model as a three dimensional Gaussian with width σ centered on the respective lattice sites.

Since the long-ranged exchange interactions $\bar{V}$ (given by (3)) are functions of the separation between the atoms, the uncertainty in the atomic positions translates into disorder in the hopping rates in the exchange Hamiltonian H given by equation (2). This kind of positional disorder in Hamiltonians with long-ranged hopping has been recently studied and found to give rise to localization [47]. Consistently with this, we find that as we increase σ the eigenstates of the Hamiltonian become localized, inhibiting transport. This can be seen in the top panels of figures 6(a)–(c), where we show the excitation probability $|c_\alpha^0(t)|^2$ as a function of time for increasing disorder (ratio σ/a) from left to right.

Subradiance is, however, not a fine-tuned property but rather known to be robust in the presence of disorder [49, 50]. Indeed, in each lower panel in figures 6(a)–(c) one can observe that, while increasing disorder has a detrimental effect on the subradiant state manifold, in all cases considered the excitation features lifetimes dramatically longer than the ones of an individual atom.

6. Conclusions and outlook

We have investigated the transport of an excitation in a one-dimensional atomic lattice that occurs due to the coupling of the atoms to the radiation field. In particular, we have shown that there is a high dimensional subradiant manifold that allows for dispersionless transport, control and storage of wave packets.

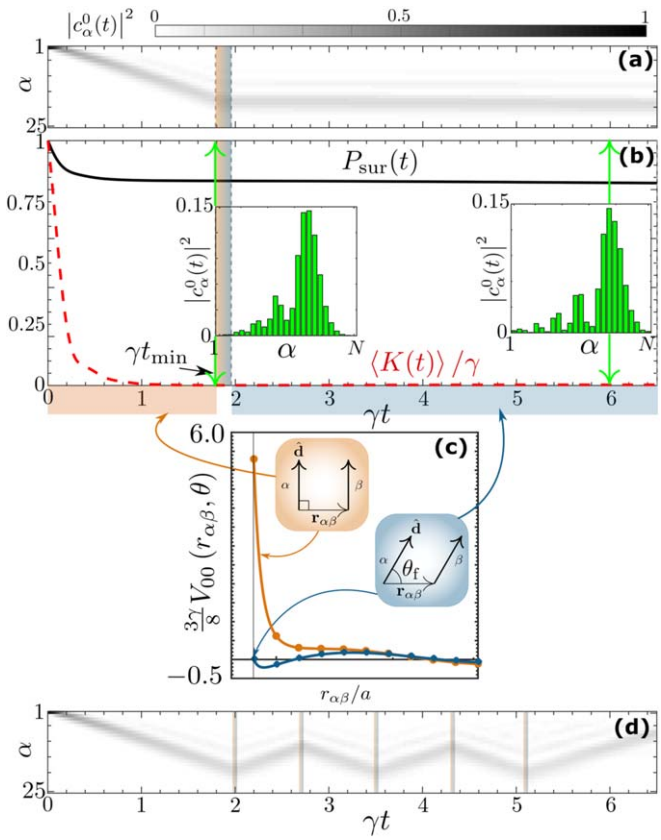

Figure 5. Excitation freezing. Dynamics of a single excitation, initially under the same conditions as figure 4. At the time when the activity is minimized, $t_{\rm min}$, the magnetic field ($\Delta = 10^3\gamma$) is rotated adiabatically (orange-blue shaded region between dashed lines) to the optimal angle for storage $\theta_{\rm f}$. (a) Excitation probability $|c^0_\alpha(t)|^2$ at each site α as a function of time. (b) Survival probability $P_{\rm sur}(t)$ (solid black) and activity $\langle K(t)\rangle/\gamma$ (dashed red) as a function of time. The insets show individual atom populations at $\gamma t_{\rm min} = 1.79$ and $\gamma t = 6$. (c) Interaction strengths in the 1D chain between two atoms in the $|0\rangle$ state: at $t = 0$, with the dipole moments of the atoms aligned perpendicular to the atom separation (orange) and after the change of direction of the magnetic field, when the dipole moments have followed the change adiabatically and are aligned at an angle $\theta_{\rm f}$ in order to minimize the coupling between nearest neighbors (blue). (d) Excitation probability $|c^0_\alpha(t)|^2$ at each site α as a function of time, where the magnetic field is repeatedly switched from $\pi/2$ to an angle where the nearest neighbor interactions change sign and viceversa.

However, there are a number of experimental challenges to overcome when considering the realization of such long lived excitation storage in a dissipative system. One is to achieve a sufficiently small ratio a/λ such that highly subradiant states emerge. An example of such a system, using a transition in the triplet series of alkaline earth metal atoms with a particularly long wavelength (2.6 μm in strontium), was introduced in [4]. With a single atom decay rate of $\gamma = 290$ kHz, a chain of strontium atoms would require quite fast switching times τ for the magnetic field direction of the order of microseconds or tens of microsenconds (longer switching times are possible for a larger system size and ratio a/λ, as the excitation takes longer to leave the bulk). The trapping of these alkaline earth metal atoms is currently realized experimentally both in optical lattices [52, 53] and tweezer arrays [54]. Even smaller ratios a/λ can be achieved by using Rydberg states, where the transition wavelengths are much longer than in low-lying states. An alternative approach that allows subradiant states to emerge for large ratios a/λ is changing the radiation field's boundary conditions by placing, e.g. a surface or a waveguide [33, 55–62] near the atoms, which in turn modifies the exchange interaction and dissipation. Another experimental challenge is the preparation of the subradiant wave packets. In particular, preparing states with one excitation localized on one or a few sites will require single-site resolution and addressability, which has been achieved experimentally in optical lattices and tweezer arrays [63–67]. Moreover, creating a wave packet with a linear dispersion relation will require a phase imprinting mechanism, which may be challenging to implement experimentally.

A future direction connecting to this work will be to move away from the linear optics regime (single excitation sector of the dynamics) [33, 35, 37, 38, 68] and consider situations where two or more wave packets interfere with each other effectively realizing photon–photon interactions in a subradiant decoherence-free

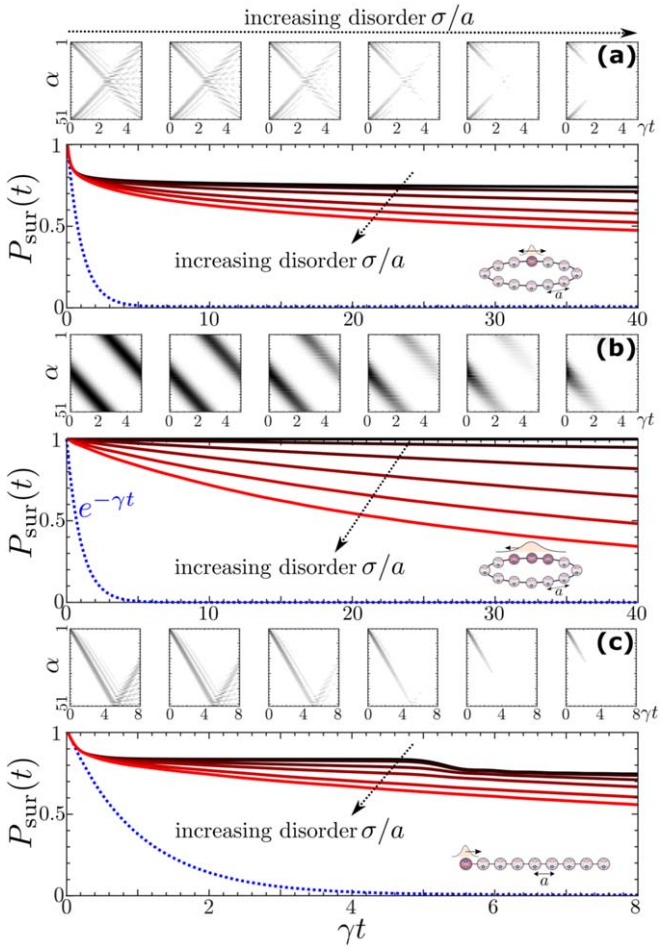

Figure 6. Disorder. Survival probability for an initial excitation on a chain of $N = 51$ atoms and $a/\lambda = 0.08$ (a) on a single site on a ring lattice, (b) on an extended gaussian wave packet on a ring lattice and (c) on a single site on a linear 1D lattice. All panels show the excitation probability $|c_\alpha^0(t)|^2$ at site α as a function of time and the survival probability without disorder (leftmost panel, black solid line) and in the presence of disorder (rest of panels and solid red lines), modeled by a gaussian distribution of the positions of the atoms around the center of each site with widths $\sigma = 0.01a \rightarrow 0.05a$ (average over 100 iterations of the disorder). The blue dashed line in all cases represents an exponential decay with single atom decay rate γ for comparison.

manifold. Such platforms can find applications ranging from the creation of non-classical states of light to the realization of photon–photon quantum gates [69, 70].

Acknowledgments

The authors acknowledge fruitful discussions with Katarzyna Macieszczak, Matteo Marcuzzi, and Thomas Fernholz. BO was supported by the Royal Society and EPSRC [Grant No. DH130145]. The research leading to these results has received funding from the European Research Council under the European Union's Seventh Framework Programme (FP/2007-2013) [ERC Grant Agreement No. 335266 (ESCQUMA)] and from the European Union's H2020 research and innovation programme [Grant Agreement No. 800942 (ErBeStA)]. Funding was also received from the EPSRC [Grant No. EP/M014266/1 and No. EP/R04340X/1]. IL gratefully acknowledges funding through the Royal Society Wolfson Research Merit Award.

Appendix. Dynamics in the truncated Hilbert space

In this appendix we give the expressions for the equations of motion of each component of the truncated density matrix (8). We obtain these equations by simply substituting the expression (8) into the master equation (1), such that we can split the density matrix into the four components $\rho_{GG} = \langle G|\rho|G\rangle$, $\rho_{Ge_\alpha^m} = \langle G|\rho|e^m\rangle_\alpha$, $\rho_{e_\alpha^m G} = {}_\alpha\langle e^m|\rho|G\rangle$ and $\rho_{e_\alpha^m e_\beta^l} = {}_\alpha\langle e^m|\rho|e^l\rangle_\beta$. The time evolution of each component is given by

$$\dot{\rho}_{GG} = \sum_{\gamma\epsilon}\sum_{np}\Gamma^{np}_{\gamma\epsilon}\rho_{e^n_\gamma e^p_\epsilon}$$
$$\dot{\rho}_{Ge^m_\alpha} = \frac{\mathrm{i}}{\hbar}\sum_{\gamma}\sum_{n}\rho_{Ge^n_\gamma}[\hbar Z^{nm*}_{\gamma\alpha} + \Delta^{nm}_{\gamma\gamma}\delta_{\gamma\alpha}]$$
$$\dot{\rho}_{e^m_\alpha G} = -\frac{\mathrm{i}}{\hbar}\sum_{\gamma}\sum_{n}[\hbar Z^{mn}_{\alpha\gamma} + \Delta^{mn}_{\gamma\gamma}\delta_{\gamma\alpha}]\rho_{e^n_\gamma G} \tag{A1}$$

and

$$\dot{\rho}_{e^m_\alpha e^l_\beta} = -\frac{\mathrm{i}}{\hbar}\sum_{\gamma}\sum_{n}[(\hbar Z^{mn}_{\alpha\gamma} + \Delta^{mn}_{\gamma\gamma}\delta_{\gamma\alpha})\rho_{e^n_\gamma e^l_\beta} - \rho_{e^m_\alpha e^n_\gamma}(\hbar Z^{nl*}_{\gamma\beta} + \Delta^{nl}_{\gamma\gamma}\delta_{\gamma\beta})], \tag{A2}$$

where $Z^{ml}_{\alpha\beta} = V^{ml}_{\alpha\beta} - \frac{\mathrm{i}}{2}\Gamma^{ml}_{\alpha\beta}$ (equations (3) and (7)).

ORCID iDs

Igor Lesanovsky https://orcid.org/0000-0001-9660-9467
Beatriz Olmos https://orcid.org/0000-0002-1140-2641

References

[1] Dicke R H 1954 Coherence in spontaneous radiation processes *Phys. Rev.* **93** 99
[2] Lehmberg R H 1970 Radiation from an N-atom system: I. General formalism *Phys. Rev.* A **2** 883
[3] Agarwal G S 1971 Master-equation approach to spontaneous emission: II. Emission from a system of harmonic oscillators *Phys. Rev.* A **3** 1783
[4] Olmos B, Yu D, Singh Y, Schreck F, Bongs K and Lesanovsky I 2013 Long-range interacting many-body systems with alkaline-earth-metal atoms *Phys. Rev. Lett.* **110** 143602
[5] Sutherland R T and Robicheaux F 2016 Collective dipole–dipole interactions in an atomic array *Phys. Rev.* A **94** 013847
[6] Bettles R J, Gardiner S A and Adams C S 2016 Cooperative eigenmodes and scattering in one-dimensional atomic arrays *Phys. Rev.* A **94** 043844
[7] Friedberg R, Hartmann S and Manassah J 1973 Frequency shifts in emission and absorption by resonant systems ot two-level atoms *Phys. Rep.* **7** 101
[8] Scully M O 2009 Collective Lamb shift in single photon Dicke superradiance *Phys. Rev. Lett.* **102** 143601
[9] Keaveney J, Sargsyan A, Krohn U, Hughes I G, Sarkisyan D and Adams C S 2012 Cooperative Lamb shift in an atomic vapor layer of nanometer thickness *Phys. Rev. Lett.* **108** 173601
[10] Pellegrino J, Bourgain R, Jennewein S, Sortais Y R, Browaeys A, Jenkins S D and Ruostekoski J 2014 Observation of suppression of light scattering induced by dipole–dipole interactions in a cold-atom ensemble *Phys. Rev. Lett.* **113** 133602
[11] Jenkins S D, Ruostekoski J, Javanainen J, Jennewein S, Bourgain R, Pellegrino J, Sortais Y R P and Browaeys A 2016 Collective resonance fluorescence in small and dense atom clouds: comparison between theory and experiment *Phys. Rev.* A **94** 023842
[12] Bromley S L *et al* 2016 Collective atomic scattering and motional effects in a dense coherent medium *Nat. Commun.* **7** 11039
[13] Peyrot T, Sortais Y R P, Browaeys A, Sargsyan A, Sarkisyan D, Keaveney J, Hughes I G and Adams C S 2018 Collective Lamb shift of a nanoscale atomic vapor layer within a sapphire cavity *Phys. Rev. Lett.* **120** 243401
[14] Bienaimé T, Piovella N and Kaiser R 2012 Controlled Dicke subradiance from a large cloud of two-level systems *Phys. Rev. Lett.* **108** 123602
[15] Ott J R, Wubs M, Lodahl P, Mortensen N A and Kaiser R 2013 Cooperative fluorescence from a strongly driven dilute cloud of atoms *Phys. Rev.* A **87** 061801
[16] de Oliveira R A, Mendes M S, Martins W S, Saldanha P L, Tabosa J W R and Felinto D 2014 Single-photon superradiance in cold atoms *Phys. Rev.* A **90** 023848
[17] Guerin W, Araújo M O and Kaiser R 2016 Subradiance in a large cloud of cold atoms *Phys. Rev. Lett.* **116** 083601
[18] Araújo M O, Krešić I, Kaiser R and Guerin W 2016 Superradiance in a large and dilute cloud of cold atoms in the linear-optics regime *Phys. Rev. Lett.* **117** 073002
[19] Roof S J, Kemp K J, Havey M D and Sokolov I M 2016 Observation of single-photon superradiance and the cooperative Lamb shift in an extended sample of cold atoms *Phys. Rev. Lett.* **117** 073003
[20] Araújo M O, Guerin W and Kaiser R 2018 Decay dynamics in the coupled-dipole model *J. Mod. Opt.* **65** 1345
[21] Cottier F, Kaiser R and Bachelard R 2018 Role of disorder in super- and subradiance of cold atomic clouds *Phys. Rev.* A **98** 013622
[22] Filipp S, van Loo A F, Baur M, Steffen L and Wallraff A 2011 Preparation of subradiant states using local qubit control in circuit qed *Phys. Rev.* A **84** 061805
[23] Lalumière K, Sanders B C, van Loo A F, Fedorov A, Wallraff A and Blais A 2013 Input–output theory for waveguide qed with an ensemble of inhomogeneous atoms *Phys. Rev.* A **88** 043806
[24] Jenkins S D, Ruostekoski J, Papasimakis N, Savo S and Zheludev N I 2017 Many-body subradiant excitations in metamaterial arrays: experiment and theory *Phys. Rev. Lett.* **119** 053901
[25] Lodahl P, Floris van Driel A, Nikolaev I S, Irman A, Overgaag K, Vanmaekelbergh D and Vos W L 2004 Controlling the dynamics of spontaneous emission from quantum dots by photonic crystals *Nature* **430** 654
[26] Tighineanu P, Daveau R S, Lehmann T B, Beere H E, Ritchie D A, Lodahl P and Stobbe S 2016 Single-photon superradiance from a quantum dot *Phys. Rev. Lett.* **116** 163604
[27] Kim J-H, Aghaeimeibodi S, Richardson C J K, Leavitt R P and Waks E 2018 Super-radiant emission from quantum dots in a nanophotonic waveguide *Nano Lett.* **18** 4734
[28] Scully M O, Fry E S, Ooi C H R and Wódkiewicz K 2006 Directed spontaneous emission from an extended ensemble of n atoms: timing is everything *Phys. Rev. Lett.* **96** 010501

[29] Plankensteiner D, Ostermann L, Ritsch H and Genes C 2015 Selective protected state preparation of coupled dissipative quantum emitters *Sci. Rep.* **5** 16231
[30] Scully M O 2015 Single photon subradiance: quantum control of spontaneous emission and ultrafast readout *Phys. Rev. Lett.* **115** 243602
[31] Jen H H, Chang M S and Chen Y C 2016 Cooperative single-photon subradiant states *Phys. Rev.* A **94** 013803
[32] Facchinetti G, Jenkins S D and Ruostekoski J 2016 Storing light with subradiant correlations in arrays of atoms *Phys. Rev. Lett.* **117** 243601
[33] Asenjo-Garcia A, Moreno-Cardoner M, Albrecht A, Kimble H J and Chang D E 2017 Exponential improvement in photon storage fidelities using subradiance and 'selective radiance' in atomic arrays *Phys. Rev.* X **7** 031024
[34] Jen H H 2017 Phase-imprinted multiphoton subradiant states *Phys. Rev.* A **96** 023814
[35] Jen H H 2018 Directional subradiance from helical-phase-imprinted multiphoton states *Sci. Rep.* **8** 7163
[36] Jen H H, Chang M-S and Chen Y-C 2018 Cooperative light scattering from helical-phase-imprinted atomic rings *Sci. Rep.* **8** 9570
[37] Moreno-Cardoner M, Plankensteiner D, Ostermann L, Chang D and Ritsch H 2019 Extraordinary subradiance with lossless excitation transfer in dipole-coupled nano-rings of quantum emitters arXiv:1901.10598
[38] Guimond P-O, Grankin A, Vasilyev D V, Vermersch B and Zoller P 2019 Subradiant bell states in distant atomic arrays *Phys. Rev. Lett.* **122** 093601
[39] Bettles R J, Minář J C V, Adams C S, Lesanovsky I and Olmos B 2017 Topological properties of a dense atomic lattice gas *Phys. Rev.* A **96** 041603
[40] Perczel J, Borregaard J, Chang D E, Pichler H, Yelin S F, Zoller P and Lukin M D 2017 Topological quantum optics in two-dimensional atomic arrays *Phys. Rev. Lett.* **119** 023603
[41] Willingham B and Link S 2011 Energy transport in metal nanoparticle chains via sub-radiant plasmon modes *Opt. Express* **19** 6450
[42] Giusteri G G, Mattiotti F and Celardo G L 2015 Non-Hermitian Hamiltonian approach to quantum transport in disordered networks with sinks: validity and effectiveness *Phys. Rev.* B **91** 094301
[43] Leggio B, Messina R and Antezza M 2015 Thermally activated nonlocal amplification in quantum energy transport *Europhys. Lett.* **110** 40002
[44] Doyeux P, Messina R, Leggio B and Antezza M 2017 Excitation injector in an atomic chain: long-range transport and efficiency amplification *Phys. Rev.* A **95** 012138
[45] Doyeux P, Gangaraj S A H, Hanson G W and Antezza M 2017 Giant interatomic energy-transport amplification with nonreciprocal photonic topological insulators *Phys. Rev. Lett.* **119** 173901
[46] Mattioni A, Caycedo-Soler F, Huelga S F and Plenio M B 2018 Design principles for long-range energy transfer at room temperature arXiv:1812.07905
[47] Deng X, Kravtsov V E, Shlyapnikov G V and Santos L 2018 Duality in power-law localization in disordered one-dimensional systems *Phys. Rev. Lett.* **120** 110602
[48] Botzung T, Vodola D, Naldesi P, Müller M, Ercolessi E and Pupillo G 2018 Algebraic localization from power-law interactions in disordered quantum wires arXiv:1810.09779
[49] Akkermans E and Gero A 2013 Cooperative effects in one-dimensional random atomic gases: absence of single-atom limit *Europhys. Lett.* **101** 54003
[50] Biella A, Borgonovi F, Kaiser R and Celardo G L 2013 Subradiant hybrid states in the open 3d Anderson–Dicke model *Europhys. Lett.* **103** 57009
[51] James D F 1993 Frequency shifts in spontaneous emission from two interacting atoms *Phys. Rev.* A **47** 1336
[52] Yamamoto R, Kobayashi J, Kuno T, Kato K and Takahashi Y 2016 An ytterbium quantum gas microscope with narrow-line laser cooling *New J. Phys.* **18** 023016
[53] Miranda M, Inoue R, Tambo N and Kozuma M 2017 Site-resolved imaging of a bosonic Mott insulator using ytterbium atoms *Phys. Rev.* A **96** 043626
[54] Norcia M A, Young A W and Kaufman A M 2018 Microscopic control and detection of ultracold strontium in optical-tweezer arrays *Phys. Rev.* X **8** 041054
[55] Le Kien F and Rauschenbeutel A 2017 Nanofiber-mediated chiral radiative coupling between two atoms *Phys. Rev.* A **95** 023838
[56] Lodahl P, Mahmoodian S, Stobbe S, Rauschenbeutel A, Schneeweiss P, Volz J, Pichler H and Zoller P 2017 Chiral quantum optics *Nature* **541** 473
[57] Gangaraj S A H, Hanson G W and Antezza M 2017 Robust entanglement with three-dimensional nonreciprocal photonic topological insulators *Phys. Rev.* A **95** 063807
[58] Jones R, Needham J A, Lesanovsky I, Intravaia F and Olmos B 2018 Modified dipole–dipole interaction and dissipation in an atomic ensemble near surfaces *Phys. Rev.* A **97** 053841
[59] Buonaiuto G, Jones R, Olmos B and Lesanovsky I 2019 Dynamical creation and detection of entangled many-body states in a chiral atom chain arXiv:1902.08525
[60] Albrecht A, Henriet L, Asenjo-Garcia A, Dieterle P B, Painter O and Chang D E 2019 Subradiant states of quantum bits coupled to a one-dimensional waveguide *New J. Phys.* **21** 025003
[61] Jen H H 2019 Selective transport of atomic excitations in a driven chiral-coupled atomic chain *J. Phys. B: At. Mol. Opt. Phys.* **52** 065502
[62] Jen H H, Chang M-S, Lin G-D and Chen Y-C 2019 Subradiance dynamics in a singly-excited chiral-coupled atomic chain arXiv:1905.00558
[63] Weitenberg C, Endres M, Sherson J F, Cheneau M, Schau P, Fukuhara T, Bloch I and Kuhr S 2011 Single-spin addressing in an atomic Mott insulator *Nature* **471** 319
[64] Kim H, Lee H-G, Lee W J, Jo H, Song Y and Ahn J 2016 *In situ* single-atom array synthesis using dynamic holographic optical tweezers *Nat. Commun.* **7** 13317
[65] Endres M, Bernien H, Keesling A, Levine H, Anschuetz E R, Krajenbrink A, Senko C, Vuletic V, Greiner M and Lukin M D 2016 Atom-by-atom assembly of defect-free one-dimensional cold atom arrays *Science* **354** 1024
[66] Barredo D, de Léséleuc S, Lienhard V, Lahaye T and Browaeys A 2016 An atom-by-atom assembler of defect-free arbitrary two-dimensional atomic arrays *Science* **354** 1021
[67] Cooper A, Covey J P, Madjarov I S, Porsev S G, Safronova M S and Endres M 2018 Alkaline-earth atoms in optical tweezers *Phys. Rev.* X **8** 041055
[68] Zhang Y-X and Mølmer K 2019 Theory of subradiant states of a one-dimensional two-level atom chain arXiv:1812.09784
[69] Gorshkov A V, Otterbach J, Fleischhauer M, Pohl T and Lukin M D 2011 Photon–photon interactions via Rydberg blockade *Phys. Rev. Lett.* **107** 133602
[70] Tiarks D, Schmidt-Eberle S, Stolz T, Rempe G and Dürr S 2019 A photon–photon quantum gate based on Rydberg interactions *Nat. Phys.* **15** 124